Electro-mechanical transmission modelling for series-hybrid tracked tanks

Electro-Mechanical Transmission Modelling for Series-Hybrid Tracked Tanks

Enrico Galvagno, Enzo Rondinelli
and Mauro Velardocchia
Dipartimento di Meccanica, Politecnico di Torino,
Corso Duca degli Abruzzi 24, 10129 Torino, Italy
E-mail: enrico.galvagno@polito.it
E-mail: enzo.rondinelli@polito.it
E-mail: mauro.velardocchia@polito.it

Abstract: This paper describes a mathematical model and presents the dynamic analysis of a series-hybrid tracked tank driven by two electric motors, one devoted to propulsion (PM) and the other to steering (SM). A double differential mechanism is adopted to electrically produce the speed difference between the tracks required for skid steering. In this paper this specific transmission is called Electro-Mechanical Transmission (EMT). The EMT model supports the steering motor control strategy definition and the electric motor size optimization. Dynamic simulations applied to a 55 ton Main Battle Tank are shown and discussed in order to validate the obtained results.

Keywords: military vehicle; hybrid vehicles; electro-mechanical transmission; tank; driveline; tracked vehicle modelling; skid steering.

1 Introduction

Interest in hybrid and all-electric military vehicles has increased over recent years. In the military field, research on electric vehicles is driven above all by stealth potential (silent movement), improved fuel economy (25-30%), improved accelerations, integration with electric weapons, ability of on-board power generation, reduced maintenance and flexibility in traction system layout which may help to improve ballistic protection, as discussed in the NATO Task Group AVT-047 (2004) report.
Although up to now tanks are exclusively driven by diesel engines in combination with automatic transmissions, there are several potential benefits in powertrain electrification/hybridization (Guenter, 2007). In particular, propulsion systems conceived to save energy while maintaining the required steering and traction performance are of relevant interest for tracked vehicles, especially considering how critical and expensive the fuel availability can be during a military mission. Despite the fact that, in tracked vehicles, high rolling resistance does not allow a great amount of energy to be regenerated, an energy storage device can be used to maximize overall powertrain efficiency, improve vehicle acceleration and increase the energy available to supply electrical equipment.
In a tracked vehicle the transmission system is involved in both braking and steering manoeuvres. There are various types of steering mechanism available for tracked

vehicles using the principle of skid-steering. Typically, some types of double differential mechanisms, usually controlled by mechanical components, such as clutches and brakes, can be employed to generate the required relative speed between tracks. The adoption of electric motors instead of these dissipative components allows some energy saving potentialities to be introduced.
Among the available electric powertrain schemes, two interesting solutions are the zero-shaft type steering system and a purely electric two-sprocket drive system. The first one maintains a mechanical link between the wheels, while the second one is based on two mechanically independent electric motors, one for each final drive. Although the two-electric sprocket systems appear to save space, due to the absence of several mechanical components, the specific tracked vehicles' need for both traction and steering capability leads to higher power requirements. A zero-shaft system requires lower electric motor power rating for the same steering and traction performance as shown by Hirt, M. and Naunheimer, H. (1999).
The Electro-Mechanical Transmission (EMT) considered in this paper is characterized by a zero-shaft steering system, which allows to transfer the drive power from one drive side to the other via two steering differential gears. The zero shaft can be driven from a power fraction branched off from the drive system and a steering electric motor. Some mechanical and hydrostatic arrangement variants using analogous steering principles are presented by Witzenberger, M. and Rothfisher, G. (2007). The EMT layout allows the energy required for steering to be reduced in comparison with pure mechanical solutions (brakes and clutches) and allows electric motor downsizing in comparison with a purely electric drive sprocket solution.
The optimisation of electric motor size needs an accurate estimation of forces and moments due to track-terrain interaction; as suggest by Maclaurin (2007), in this paper the distributed contact is discretised along the length of the tracks based on a number of contact patches that are equal to the number of roadwheels. A reliable EMT dynamic model can support the electric motor control strategy definition. Furthermore, the integration of EMT and tracked vehicle models constitutes an instrument to estimate the power flows through the transmission and the vehicle energy requirement for both propulsion and steering systems.

2 Description of the Electro-Mechanical Transmission (EMT)

Figure 1 shows a block diagram of the whole powertrain of a tracked vehicle equipped with the EMT. A *Power Generator* block consists of an internal combustion engine, typically a diesel engine in heavy track-laying vehicles, coupled with an electric generator. The generated power is used to supply the whole electrical load of the tank.
A detailed description of the EMT, its components, and the working principle is carried out with reference to Figure 2. The Propulsion Motor (*PM*) acts on the driven shafts via Planetary Gear Set 1 (*PGS1*) and two steering differentials indicated as *PGS2* and *PGS6*. The output shafts of the steering differentials are connected to sprockets (*WL* and *WR*) through a final speed reduction, indicated as *Final drive* in Figure 1 and omitted in Figure 5, with the aim of increasing caterpillar track forces. The steering differentials are driven by the drive system via their ring gears and the additional revolutions required for steering the vehicle are obtained through sun gear rotation. The shaft driven by the steering motor is called Zero-Shaft (*ZS*) since during straight-line events its speed is null. It forces the sun wheels of the steering differentials to rotate in opposite directions. For

this purpose an ordinary gear train (*OG5*) with two intermediate gear wheels is adopted on the left vehicle side while an ordinary gear train (*OG3*) with only one intermediate gear wheel is introduced on the right side. In this way it is possible to accelerate one track and slow down the other, thus allowing the steering manoeuvre according to the skid steering principle. Two friction brakes *Br,L* and *Br,R*, placed between the steering differentials and the final drives, allow the vehicle speed to be reduced and also the tracked tank to be steered if they generate different braking torques for the two vehicle sides.
The system composed of a gear set *PGS1*, clutch *CL*, and brake *B1* realizes a two-speed Automatic Transmission (*AT*). The first drive range of the AT is obtainable by engaging brake *B1* (*CL* must be disengaged) and is useful on difficult terrains, while the second speed is a direct drive obtainable by engaging the clutch *CL* (*B1* must be disengaged) and is suitable for easy terrains and roadways.
Table 1 shows the gear ratios of the two-speed AT.

3 Dynamic model

3.1 General description

The dynamic model is composed of four main subsystems as depicted in Figure 3, named *Control*, *Electric Motors*, *Transmission* and *Tracked Vehicle*.
The *Control* subsystem contains the control logic used to calculate the reference values for both the propulsion and the steering motors, depending on the desired manoeuvre.
The *Electric Motors* block computes the torque delivered by the two electric motors according to their control signals, coming from the Control block, and depending on the saturation imposed by the respective maximum torque maps. A first order low-pass filter is introduced between the desired and the actual torque value to take into account the torque control system bandwidth.
The transmission dynamics are modelled in the *Transmission* block starting from the driving torques supplied by the actuators, the resistant torques exerted by the tracks, and the torques applied by the braking system on the brake disks.
Last main block, i.e. the *Tracked Vehicle*, has two main tasks: the mathematical description of the track-terrain interaction and the vehicle dynamics. The forces applied to the ground by the tracks are concentrated under the roadwheels and simulated using a smoothed Coulomb friction model. The vehicle motion is described by three degrees of freedom (d.o.f.): the longitudinal and lateral position of the centre of gravity and the rotation about a vertical axis (yaw angle).

3.2 Model assumptions and limitations

The principal assumptions made and the consequent model limitations are:
- rigid transmission components, i.e. no compliance effects are considered, and no gear backlash in the transmission, hence the validity of this model is limited to steady-state and low-frequency manoeuvres;
- inertial terms concentrated in the following positions: propulsion motor (J_{PM}), steering motor (J_{SM}), sprockets (J_{WL}, J_{WR}) and vehicle (m);
- continuous track-terrain contact discretised in a finite number of contact patches equal to the number of roadwheels. Contact patch forces are modelled as smoothed friction

functions depending on the longitudinal slip and sideslip angle of the tracks, combined load operations are modelled using look-up tables;
- firm ground, the effect of sinkage is neglected;
- cohesion on the track-terrain interface is neglected;
- equal spacing between the contact patches in the longitudinal direction;
- three d.o.f. vehicle dynamics;
- transverse terrain inclination is neglected;
- longitudinal and lateral load transfer computation;
- independent wheel suspension with the same vertical stiffness for each roadwheel and a generic N number of axles; (only considered for the longitudinal load transfer calculation)
- equal ground loading in static configuration;
- aerodynamic resistance computation includes only longitudinal drag coefficient and the resultant force is considered applied to the vehicle centre of gravity;
- unitary efficiency for all the transmission components.

3.3 Transmission model

The *Transmission* model receives the following inputs: the torques supplied by the electric motors (T_{PM} , T_{SM}), the load torques acting on the tracks (T_{lR} , T_{lL}), and the braking torques ($T_{Br,R}$, $T_{Br,L}$), and gives the speeds of the two electric motors (ω_{PM} , ω_{SM}) and the sprockets speeds (ω_{WR} , ω_{WL}) as outputs.
Torques and velocities are considered positive according to the sign convention indicated in Figure 2. It must be noted that, due to usage of the same sign convention for all the internal transmission torques, auxiliary variables, indicated with an apostrophe, e.g. *T'*, were introduced during the system decomposition process into its basic components, as shown in Figure 4.
The interface equation that expresses the passage from one component to the other, according to Newton's action-reaction principle, is therefore:
$T = -T'$. These obvious equations are not reported in the paper but are needed to eliminate the internal variables and solve the system of transmission dynamic equations.
The free body diagrams used to determine the transmission motion equations are shown in Figure 4.

Motors
The dynamic torque balance about each motor shaft gives:

$$\dot{\omega}_M = \frac{T_M + T_{lM}}{J_M} \tag{1}$$

where $\dot{\omega}_M, T_M, T_{lM}$ and J_M are respectively the motor angular acceleration, the motor torque, the load torque and the motor moment of inertia.

Planetary gear sets
As well known, for an epicyclic gearing the three angular speeds ω_S, ω_C and ω_R, of the sun gear *S*, the planet carrier *C* and the ring gear *R* respectively, are constrained by Willis's formula:

$$\omega_S + \sigma\omega_R = (1+\sigma)\omega_C . \tag{2}$$

where $\sigma = N_R / N_S$ is the planetary gear set ratio and N_R, N_S are the number of teeth.

Under the hypothesis of unitary efficiency and neglecting the inertias of the epicyclical gear set, the torque equilibrium of the gearing yields: $\sigma = T_R / T_S$ where T_R, T_S are the ring and sun torques. The torque on the carrier T_C is related to the other torques through:

$$\begin{aligned} T_C / T_S &= -(1+\sigma) \\ T_C / T_R &= -(1+1/\sigma) \end{aligned} \tag{3}$$

Sprockets
The dynamic balance between the moments about each sprocket axis of rotation gives:

$$T_W - T_l = J_W \dot{\omega}_W \tag{4}$$

where $\dot{\omega}_W$, T_W, T_l and J_W are respectively the sprocket angular acceleration, the torque from transmission after the final drive amplification, the load torque from the vehicle and the rotary inertia of the considered sprocket.

Brakes
Under the hypothesis of negligible brake disk inertia, the brake disk equilibrium equation, for each vehicle side, is

$$T_C + T_{Br} + T_{FD} = 0 \tag{5}$$

T_C is the torque coming from the carrier of the steering differential, T_{Br} is the braking torque and $T_{FD}=T_W/\tau_{FD}$ is the final drive input torque, τ_{FD} is the final drive ratio.

Transmission motion equations
From equations (1), (3), (4), (5), by making appropriate substitutions, the following equation can be obtained for the torque on ring gear of PGS6 (subscript $_L$ stands for left):

$$T_{R6} = \frac{\dfrac{J_{WL}\dot{\omega}_{WL} + T_{lL}}{\tau_{FD}} + T_{Br,L}}{1 + \dfrac{1}{\sigma_6}} \tag{6}$$

In the same way on the right side it is possible to write:

$$T_{R2} = \frac{\dfrac{J_{WR}\dot{\omega}_{WR} + T_{lR}}{\tau_{FD}} + T_{Br,R}}{1 + \dfrac{1}{\sigma_2}} \tag{7}$$

Since the two steering differentials must be equal to allow the vehicle to ride straight ahead when no steering action is required, obviously it follows that: $\sigma_2 = \sigma_6 = \sigma_{PG}$

From the torque balance written for the lower shaft, *LS* in Figure 2, that connects the two ring gears of the steering differentials, it results:

$$T_{C1} = T_{CL} - T_{R2} - T_{R6} \tag{8}$$

As previously stated the sequence of the clutch *CL* and the planetary gear set *PGS1*, just downstream of the propulsion motor, forms a two-speed Automatic Transmission. In what follows, the AT will be considered as an ideal torque multiplication and speed reduction element of the same factor τ_{AT} :

$$\begin{aligned} &T_{CL} - T_{C1} = \left(T_{PM} - J_{PM}\dot{\omega}_{PM}\right)\tau_{AT} \\ &\omega_{C1} = \omega_{PM} / \tau_{AT} \end{aligned} \tag{9}$$

The transmission ratio τ_{AT} assumes the following values: 1 if the clutch is engaged, $1+\sigma_1$ if the brake B1 is engaged while the clutch is disengaged.
By substituting eq. (1) written for the propulsion motor and (6), (7), (9) in (8), considering a generic constant gear ratio imposed by the two-speed AT, it gives:

$$\tau_{AT}T_{PM} - \frac{\sigma_{PG}}{\sigma_{PG}+1}\left(\frac{T_{lR}+T_{lL}}{\tau_{FD}} + T_{Br,R} + T_{Br,L}\right) = \tau_{AT}J_{PM}\dot{\omega}_{PM} + \frac{\sigma_{PG}}{(\sigma_{PG}+1)\tau_{FD}}\left(J_{WR}\dot{\omega}_{WR} + J_{WL}\dot{\omega}_{WL}\right) \tag{10}$$

The torque balance on the zero shaft gives:

$$\begin{cases} T_{UP3} + T_{UP5} + T_{UP4} = 0 \\ \omega_{UP4} = \omega_{UP5} = \omega_{UP3} \end{cases} \tag{11}$$

Let us define the gear ratios of the three ordinary gear sets as follows:

$$\tau_3 = \frac{N_{DW3}}{N_{UP3}} = \frac{\omega_{UP3}}{\omega_{DW3}} = \frac{T_{DW3}}{T_{UP3}}$$

$$\tau_5 = \frac{N_{DW5}}{N_{UP5}} = -\frac{\omega_{UP5}}{\omega_{DW5}} = -\frac{T_{DW5}}{T_{UP5}} \tag{12}$$

$$\tau_4 = \tau_{SM} = \frac{N_{UP4}}{N_{DW4}} = \frac{\omega_{DW4}}{\omega_{UP4}} = \frac{T_{UP4}}{T_{DW4}}$$

The interface equations are: T_{DW3}=-T_{S2} , T_{DW5}=-T_{S6} , T_{DW4}=-$T_{l,SM}$.
The first equation of system (11) could be rewritten in terms of torque on the ring gear of the two steering differentials:

$$\frac{T_{R2}}{\tau_3\sigma_2} - \frac{T_{R6}}{\tau_5\sigma_6} + \tau_4\left(J_{SM}\dot{\omega}_{SM} - T_{SM}\right) = 0 \tag{13}$$

Consequently, the following dynamic equation, useful for the definition of steering motor control strategy, can be obtained:

$$T_{SM} - \frac{\left(T_{lL} - T_{lR}\right)/\tau_{FD} + T_{Br,L} - T_{Br,R}}{\tau_{OG}\tau_{SM}(\sigma_{PG}+1)} = J_{SM}\dot{\omega}_{SM} + \frac{J_{WR}\dot{\omega}_{WR} - J_{WL}\dot{\omega}_{WL}}{\tau_{FD}\tau_{OG}\tau_{SM}(\sigma_{PG}+1)} \tag{14}$$

where $\tau_{OG} = \tau_3 = \tau_5$ from the hypothesis of the symmetry of the transmission system. Eqs. (10) and (14) are the dynamic equations of the transmission. The transmission kinematic equations can be written considering first of all that $\omega_{R6} = \omega_{R2} = \omega_{C1} = \omega_{PM} / \tau_{AT}$ being the propulsion motor connected to the carrier of PGS1 through the AT. In addition $\omega_{WL} = \omega_{C6} / \tau_{FD}$ and $\omega_{WR} = \omega_{C2} / \tau_{FD}$, then:

$$\omega_{WL} = \frac{\frac{\sigma_{PG}}{\tau_{\mathrm{AT}}}\omega_{PM} - \frac{\omega_{SM}}{\tau_{SM}\tau_{OG}}}{\tau_{FD}(1+\sigma_{PG})}; \quad \omega_{WR} = \frac{\frac{\sigma_{PG}}{\tau_{\mathrm{AT}}}\omega_{PM} + \frac{\omega_{SM}}{\tau_{SM}\tau_{OG}}}{\tau_{FD}(1+\sigma_{PG})} \tag{15}$$

The latter equations highlight that a positive steering motor speed (i.e. $\omega_{SM} > 0$) increases the speed of the right sprocket and slows down the other one. The steering motor is responsible for differentiating the speeds of the two sprockets. The speed difference between the sprockets is:

$$\Delta\omega_W = \omega_{WR} - \omega_{WL} = \frac{2}{\tau_{FD}\tau_{OG}\tau_{SM}(1+\sigma_{PG})}\omega_{SM} \tag{16}$$

Moreover it is also possible to observe that during straight line maneuvers the steering motor speed must be null, thereby determining the so-called zero-shaft operating mode, in order to allow both the wheels to rotate at the same speed.

From (15) the expressions of the speeds of the two motors can be derived:

$$\begin{cases} \omega_{PM} = \dfrac{\tau_{FD}\tau_{AT}(\sigma_{PG}+1)}{2\sigma_{PG}}(\omega_{WL}+\omega_{WR}) \\ \omega_{SM} = \dfrac{\sigma_{PG}+1}{2}\tau_{FD}\tau_{SM}\tau_{OG}(\omega_{WR}-\omega_{WL}) \end{cases} \tag{17}$$

It has therefore been demonstrated that the PM speed is proportional to the mean value of the two sprocket speeds while the steering motor speed is proportional to their difference. By calculating the time derivatives of equations (17) and substituting them in equations (10) and (14) it follows that:

$$\begin{cases} \tau_{AT}T_{PM} - \dfrac{\sigma_{PG}}{\sigma_{PG}+1}\left(\dfrac{T_{lR}+T_{lL}}{\tau_{FD}} + T_{Br,R} + T_{Br,L}\right) = \left(\dfrac{\sigma_{PG}+1}{2\sigma_{PG}}J_{PM}\tau_{AT}^2\tau_{FD} + \dfrac{\sigma_{PG}}{\tau_{FD}(\sigma_{PG}+1)}J_{WL}\right)\dot{\omega}_{WL} + \\ + \left(\dfrac{\sigma_{PG}+1}{2\sigma_{PG}}J_{PM}\tau_{AT}^2\tau_{FD} + \dfrac{\sigma_{PG}}{\tau_{FD}(\sigma_{PG}+1)}J_{WR}\right)\dot{\omega}_{WR} \\ T_{SM} - \dfrac{\frac{T_{lL}-T_{lR}}{\tau_{FD}} + T_{Br,L} - T_{Br,R}}{\tau_{OG}\tau_{SM}(\sigma_{PG}+1)} = \left(\dfrac{\sigma_{PG}+1}{2}\tau_{OG}\tau_{SM}\tau_{FD}J_{SM} + \dfrac{J_{WR}}{\tau_{OG}\tau_{FD}\tau_{SM}(\sigma_{PG}+1)}\right)\dot{\omega}_{WR} + \\ - \left(\dfrac{\sigma_{PG}+1}{2}\tau_{OG}\tau_{FD}\tau_{SM}J_{SM} + \dfrac{J_{WL}}{\tau_{OG}\tau_{SM}\tau_{FD}(\sigma_{PG}+1)}\right)\dot{\omega}_{WL} \end{cases} \tag{18}$$

Considering $J_{WL} = J_{WR} = J_W$ the former equations can be further simplified as follows:

$$\begin{cases} \tau_{AT} T_{PM} - \dfrac{\sigma_{PG}}{\sigma_{PG}+1}\left(\dfrac{T_{lR}+T_{lL}}{\tau_{FD}} + T_{Br,R} + T_{Br,L}\right) = \left(\dfrac{\sigma_{PG}+1}{2\sigma_{PG}} J_{PM} \tau_{AT}^2 + \dfrac{\sigma_{PG}}{\sigma_{PG}+1} J_W / \tau_{FD}{}^2\right)\left(\dot{\omega}_{WL} + \dot{\omega}_{WR}\right)\tau_{FD} \\ T_{SM} - \dfrac{\dfrac{T_{lL}-T_{lR}}{\tau_{FD}} + T_{Br,L} - T_{Br,R}}{\tau_{OG}\tau_{SM}(\sigma_{PG}+1)} = \left(\dfrac{\sigma_{PG}+1}{2} J_{SM} \tau_{OG} \tau_{SM} + \dfrac{J_W / \tau_{FD}{}^2}{\tau_{OG}\tau_{SM}(\sigma_{PG}+1)}\right)\left(\dot{\omega}_{WR} - \dot{\omega}_{WL}\right)\tau_{FD} \end{cases} \tag{19}$$

It is interesting to highlight, from the previous equations, that the PM torque amplified by the AT ratio contributes to accelerating both wheels, while the wheel acceleration difference can be obtained both by acting on the SM torque and by differentiating the braking action between the two sides of the vehicle.
For simulation purposes the equations to compute the left and right sprocket accelerations separately are also reported:

$$\dot{\omega}_{WR} = \frac{1}{2}\left[\frac{\tau_{AT} T_{PM} - \dfrac{\sigma_{PG}}{\sigma_{PG}+1}\left(\dfrac{T_{lL}+T_{lR}}{\tau_{FD}} + T_{Br,L} + T_{Br,R}\right)}{\tau_{AT}^2 \dfrac{\sigma_{PG}+1}{2\sigma_{PG}} J_{PM} + \dfrac{\sigma_{PG}}{\sigma_{PG}+1} J_W / \tau_{FD}^2} + \right.$$
$$\left. + \frac{T_{SM} - \dfrac{\dfrac{T_{lL}-T_{lR}}{\tau_{FD}} + T_{Br,L} - T_{Br,R}}{\tau_{OG}\tau_{SM}(\sigma_{PG}+1)}}{\dfrac{\sigma_{PG}+1}{2}\tau_{OG}\tau_{SM} J_{SM} + \dfrac{J_W / \tau_{FD}^2}{\tau_{OG}\tau_{SM}(\sigma+1)}}\right] \tag{20}$$

$$\dot{\omega}_{WL} = \frac{1}{2}\left[\frac{\tau_{AT} T_{PM} - \dfrac{\sigma_{PG}}{\sigma_{PG}+1}\left(\dfrac{T_{lL}+T_{lR}}{\tau_{FD}} + T_{Br,L} + T_{Br,R}\right)}{\tau_{AT}^2 \dfrac{\sigma_{PG}+1}{2\sigma_{PG}} J_{PM} + \dfrac{\sigma_{PG}}{\sigma_{PG}+1} J_W / \tau_{FD}^2} + \right.$$
$$\left. - \frac{T_{SM} - \dfrac{\dfrac{T_{lL}-T_{lR}}{\tau_{FD}} + T_{Br,L} - T_{Br,R}}{\tau_{OG}\tau_{SM}(\sigma_{PG}+1)}}{\dfrac{\sigma_{PG}+1}{2}\tau_{OG}\tau_{SM} J_{SM} + \dfrac{J_W / \tau_{FD}^2}{\tau_{OG}\tau_{SM}(\sigma_{PG}+1)}}\right] \tag{21}$$

The braking torque model adopted is:

$$T_{Br} = cT_{Br,\max} \tanh \frac{3\omega_W}{\Delta\omega_{th}} \tag{22}$$

where $T_{Br,\max}$ is the maximum braking torque, c is the percentage of the brake actuation, $\Delta\omega_{th}$ is the speed threshold to distinguish the transition from static to dynamic friction. The load on each sprocket is finally given by the sum of the rolling resistances T_{roll} and the torque generated by the interaction between terrain and caterpillar track T_{track}

$$T_l = T_{roll} + T_{track} \tag{23}$$

Rolling resistance torques assume the following expression:

$$T_{roll,L/R} = \sum_{i=1}^{N} F_{z,i,L/R}\left[f_0 + k\left(\omega_{W,L/R}R\right)^2\right]R \tanh \frac{3\omega_{W,L/R}}{\omega_{W,th}} \tag{24}$$

where f_0 and k are rolling resistance coefficients, $F_{z,i}$ is the normal load of the i-th contact patch, R is the sprocket pitch radius. Subscript $_L$ or $_R$ must be used depending on the considered track. A hyperbolic tangent function is used to smooth the rolling resistance sign change; this transition can be tuned by setting the threshold $\omega_{W,th}$.
Track torques are computed from the resultant longitudinal forces exchanged between tracks and terrain:

$$T_{track,L/R} = F_{x,L/R}\,R \tag{25}$$

3.4 Tracked vehicle model

3.4.1 Tracked vehicle dynamics

Figure 5 shows two coordinate systems: the reference coordinate system (*X*,*Y*,*Z*) fixed to the ground and a moving coordinate system (*x*,*y*,*z*) attached to the vehicle Center of Gravity (*CG*). The tracked vehicle can move on the *X*-*Y* plane and its motion is described by the motion of the body-fixed frame with respect to the reference frame. The instantaneous linear velocity of the moving tank *CG* is represented by the velocity vector *V*. Let u and v be the components of *V* in the *x* and *y* directions respectively. The yaw angle and the sideslip angle are defined as ψ and β and the directional angle of the course φ is equal to $\psi + \beta$. The effect of track-terrain interaction is summarised through two resultant longitudinal forces ($F_{x,L}$ and $F_{x,R}$), two resultant lateral forces ($F_{y,L}$ and $F_{y,R}$) oriented as shown in Figure 5, and two resultant moments ($M_{Fy,L}$ and $M_{Fy,R}$) about the CG due to lateral force spatial distribution along the tracks length. Thai et al. (1999) present an alternative method to predict the steady state steering properties of a rigid suspension tracked vehicle on soft terrain based on the calculation of the distribution of longitudinal end lateral shear resistance. In Watanabe et al.(1995) a mathematical model for a four-track steering vehicle in terms of stability and steerability is presented showing also good agreement between predicted and experimental data.

Referring to the dynamic force balance along the body axis (*x* and *y* in Figure 5) together with the moment balance about the *z* axis, the equations of motion can be expressed as:

$$\begin{cases} F_{x,L} + F_{x,R} = F_{aero} + F_{incl} + m\,a_x \\ F_{y,L} + F_{y,R} = m\,a_y \\ (F_{x,R} - F_{x,L})\dfrac{L}{2} + M_{Fy,L} + M_{Fy,R} = I_Z\,\ddot{\psi} \end{cases} \tag{26}$$

where L is the distance between the centrelines of the two tracks, F_{aero} is the aerodynamic drag force, F_{incl} is the force due to longitudinal ground inclination, m is the vehicle mass and I_Z is the moment of inertia of the vehicle about the vertical axis crossing the CG.
The longitudinal a_x and lateral a_y components of vehicle acceleration have the following expressions:

$$\begin{cases} a_x = \dot{u} - v\dot{\psi} \\ a_y = \dot{v} + u\dot{\psi} \end{cases} \tag{27}$$

The steady state steering moment of the vehicle on compacted soil $M_{st} = M_{Fy,L} + M_{Fy,R}$ was supposed to overcome lateral shear resistance while lateral bulldozing resistance is neglected. The amplitude of this turning moment accounts for the non-uniform pressure distribution between tracks and terrain due to both longitudinal and lateral dynamic load transfer.

3.4.2 Track-terrain model

Contact forces and moments

Since in practice ground loading is concentrated under the roadwheels, the distributed contact between tracks and terrain is discretised into a number of contact patches equal to the number of roadwheels, as assumed also by Maclaurin (2007) and Yugang and Guangjun (2009). Considering a non-cohesive terrain, for each contact patch longitudinal and lateral forces are calculated through a hyperbolic tangent function:

$$\begin{aligned} F_{x,i} &= k_\alpha\,\mu\,F_{z,i}\tanh\left(\frac{3\,s_i}{s_{F\max}}\right) \\ F_{y,i} &= k_s\,\mu\,F_{z,i}\tanh\left(\frac{-3\,\alpha_i}{\alpha_{F\max}}\right) \end{aligned} \tag{28}$$

Both of these forces are proportional to friction coefficient μ and normal load $F_{z,i}$. It is worth noting that these normal loads can change during tests, in comparison with the static uniform distribution, due to dynamic load transfer as described in the next section. The dependence upon the longitudinal slip and sideslip angle can be easily tuned using the two thresholds $s_{F\max}$ and $\alpha_{F\max}$. In

Figure 6 the final characteristics used for simulations are reported; the threshold values are set to 30° for the sideslip and 0.3 for the longitudinal slip, according to experimental data shown by Maclaurin (2007).

Additional coefficients k_α and k_s, mapped as a function of sideslip angle and of longitudinal slip respectively, are introduced in the model to describe the effect of the track combined slip and are implemented by means of look-up tables. The resultant steady-state behavior of the track-terrain interaction for each contact patch can be summarized through a plot of lateral force vs. longitudinal force for different sideslip angles and longitudinal slip (see Figure 7).
The moments about CG due to lateral forces $F_{y,i}$ are (see Figure 8):

$$\begin{aligned} M_{Fy,Li} &= F_{y,Li}\left[a - \frac{L}{N-1}i\right] \\ M_{Fy,Ri} &= F_{y,Ri}\left[a - \frac{L}{N-1}i\right] \end{aligned} \tag{29}$$

The resultant longitudinal and lateral forces and moment about the vehicle vertical axis due to tracks-terrain interaction are the summation of the effects of singles contact patches:

$$\begin{aligned} F_{x,L} &= \sum_{i=1}^{N} F_{x,Li}\ ;\ F_{y,L} = \sum_{i=1}^{N} F_{y,Li}\ ;\ M_{Fy,L} = \sum_{i=1}^{N} M_{Fy,Li} \\ F_{x,R} &= \sum_{i=1}^{N} F_{x,Ri}\ ;\ F_{y,R} = \sum_{i=1}^{N} F_{y,Ri}\ ;\ M_{Fy,R} = \sum_{i=1}^{N} M_{Fy,Ri} \end{aligned} \tag{30}$$

More detailed track-terrain models are available in Literature that are able to predict the track motion resistance as well as the tractive effort of a track as functions of soil properties (Wong, 2010). For the sake of simplicity it was decided to use a basic model with the lowest possible number of parameters while maintaining a good level of approximation of the physical phenomenon.

Kinematics

During turning manoeuvres, the longitudinal and lateral components, i.e. u_i and v_i respectively, of individual roadwheel translational speed differ from the ones relative to the vehicle center of gravity. With reference to Figure 8 and considering the rigid body kinematics applied to the vehicle it yields:

$$\begin{cases} u_{Li} = u - \dot{\psi}\dfrac{L}{2} \\ u_{Ri} = u + \dot{\psi}\dfrac{L}{2} \end{cases} \qquad \begin{cases} v_{Li} = v + \dot{\psi}\left(a - \dfrac{t}{N-1}i\right) \\ v_{Ri} = v_{Li} \end{cases} \tag{31}$$

The longitudinal slip of a generic contact patch s_i is defined as follows:

$$s_i = \begin{cases} 1 - \dfrac{u_i}{V_t} & \text{during traction} \\ \dfrac{V_t}{u_i} - 1 & \text{during braking} \end{cases}$$

where V_t is either the left or right track chain speed depending on the considered vehicle side.
In addition, each contact patch sideslip angle can be computed using the well-known definition:

$$\alpha_i = \arctan \frac{v_i}{u_i}$$

where u_i and v_i are respectively the longitudinal and transversal speed of each roadwheel hub.

Longitudinal and lateral load transfer

To evaluate the forces exerted by the *i*-th contact patch, using eq. (28), it is necessary to complete the normal load calculation considering both longitudinal and lateral load transfer. The normal load acting on a generic contact patch during a turning manoeuvre is composed by the following three contributions: the static vehicle weight distribution due to the vehicle *CG* position and longitudinal road inclination (assumed to constant), the longitudinal load transfer due to vehicle longitudinal acceleration and aerodynamic forces and the lateral load transfer mainly due to vehicle lateral acceleration:

$$F_{z,i} = F_{st,i} + \Delta F_{lon,i} + \Delta F_{lat,i} \tag{32}$$

Assuming that the *CG* is positioned longitudinally in the middle of the contact length and without eccentricity in the transversal direction, the distribution of vehicle weight between the roadwheels, in static conditions and when the road inclination α is null, is uniform. In the presence of a grade, starting from the moment equilibrium around pole *O* and the force equilibrium in the vertical, i.e. normal to the ground, direction (see Figure 9(b)), it can be demonstrated that the first addend assumes this expression:

$$F_{st,i} = \frac{mg}{2}\left(\frac{\cos\alpha}{N} - \frac{x_i}{\sum_i^N x_i^2} h_{CG} \sin\alpha \right) \tag{33}$$

where α is the longitudinal road inclination angle (lateral inclination is assumed to be null).
Referring to Figure 9(a), being h_{CG} the CG vertical distance from the ground, the moments equilibrium equation around point *O* gives the rigid load transfer due to lateral

acceleration. This lateral load transfer is equally shared out among the contact patches of a track as all the axles are considered to have the same roll stiffness:

$$\Delta F_{lat,i} = \pm \frac{m a_y h_{CG}}{L N} \tag{34}$$

Sign + applies to the contact patches of the right track, while sign – to the ones belonging to the left track, according to the adopted sign convention.
The computation of the rigid longitudinal weight transfer would be required to solve a hyperstatic structure. For this reason pitch motion due to suspension elasticity is allowed. As illustrated in Figure 10, each roadwheel is connected to the vehicle frame through a torsion bar, that determines both a vertical force $F_{z,i}$, the normal force considered to load the contact patch, and a moment about an axis normal to a lateral view of the tank M_i . The force variations with respect to the static condition are computed as follows:

$$\Delta F_{lon,i} = F_{z,i} = k_i \Delta z_i \tag{35}$$

where k_i is the equivalent vertical stiffness of each roadwheel suspension and Δz_i the *i*-th vertical relative displacement between frame and roadwheel hub. The moment arm for the vertical stiffness computation, starting from the torsion bar stiffness, can be evaluated by analysing the specific configuration of the torsion bar in the static condition, as shown in Figure 10.
With reference to Figure 9(b), the vertical displacement Δz_i can be computed considering a generic number of axles *N* again and knowing the vehicle pitch angle ϑ :

$$\begin{aligned} \Delta z_i &= x_i \tan \vartheta \\ x_i &= a - \frac{t}{N-1} i \end{aligned} \tag{36}$$

where *a* is the longitudinal position of the *CG* measured from the axis of the front sprocket and x_i is the longitudinal position with sign (positive for the front axles, negative for the rear ones) of the *i*-th axle measured from point *O*.
The axles are considered equally spaced and the wheel hub positions, in the longitudinal direction, are considered identical for the left and right vehicle side.
The pitch angle is evaluated starting from the moment balance of the vehicle about the axis of trace *O* located on the ground, considering a pitch stiffness of the whole suspension system K_p:

$$\left(F_{aero} + m a_x\right) h_{CG} + K_p \vartheta = 0 \tag{37}$$

Considering the alternative of each contribution of the roadwheel suspension, i.e. vertical forces due to the torsion bar elasticity, the former equation becomes:

$$\left(F_{aero} + m a_x\right) h_{CG} + \sum_{i=1}^{N} F_{z,i} x_i = 0 \tag{38}$$

By substituting equations (35) and (36) in (38) and assuming small pitch angles it gives:

$$\left(F_{aero} + m a_x\right) h_{CG} + \vartheta \sum_{i=1}^{N} k_i \left(a - \frac{t}{N-1} i \right)^2 = 0 \tag{39}$$

The comparison between eq. (39)
and (37) directly gives the suspension pitch stiffness K_p:

$$K_p = \sum_{i=1}^{N} k_i \left(a - \frac{t}{N-1} i \right)^2 = N k_i \left[a^2 + t^2 \frac{(N+1)(2N+1)}{6(N-1)^2} - a t \frac{N+1}{N-1} \right] \tag{40}$$

that, once substituted in the previous equations, allows the problem of the longitudinal load transfer $\Delta F_{lon,i}$ to finally be solved.

Electric Motors

The simulated vehicle is a 53.5ton Main Battle Tank equipped with a 1.1MW-11kNm electric machine for propulsion and a 0.25MW-2kNm electric machine for skid steering; the main vehicle and powertrain data was taken from Hirt and Naunheimer (1999). Figure 11 shows the maximum torque and maximum power maps of steering and propulsion motors. To ensure that the hybrid electric tank is able to achieve the 0.84MW diesel version vehicle performance, i.e. 65 km/h of maximum speed and 60% of maximum grade, a traction diagram of the vehicle was calculated and it is shown in Figure 12. The dynamics of both actuators in terms of torque control response was approximated by a first order low-pass filter with a high cutoff frequency (100rad/s) and unitary passband gain.
The two electric motors of the transmission must be chosen in order to satisfy various vehicle performance specifications such as maximum speed, gradeability, steerability, etc. As an example, a simplified procedure for steady-state vehicle traction performance computation, starting from the PM torque map and transmission parameters, is explained in section 4. More detailed results can be gained by adopting the discussed dynamic model, that considers the track longitudinal slip required for the force generation in track-terrain interface and longitudinal load transfer. SM motor size optimisation can benefit from the usage of the dynamic model as well: in fact, SM torque and speed time histories obtained during simulations of the most critical steering tests facilitate the SM size selection. The effect of different steering control strategy calibrations can also be evaluated.

3.5 Control Logic

The reference torques for the two electric motors are computed by the control logic subsystem according to the desired vehicle manoeuvre.
Since the PM torque amplified by the AT ratio increases the mean value of the speeds of the left and right tracks, see eq. (19), its reference value can be computed starting from the requested vehicle speed. Hence, a PID controller (with gains: $K_{P,PM}$, $K_{I,PM}$, $K_{D,PM}$) is implemented for the PM torque calculation whose set-point is the desired longitudinal speed of the vehicle V_{ref}.
Conversely, the presence of a non-null SM torque increases the speed difference between the tracks, generating a steering effect on the vehicle. An analogous performance can be obtained by acting on the brake system only when differentiating the braking action between the two sides of the vehicle. The effect of the braking system action is not considered in this paper, hence both the braking torques are set to zero.
The SM controller is composed of two terms, a feed-forward part, with the aim of compensating the steady-state torque required to keep a certain vehicle yaw rate, and a PID controller (with gains: $K_{P,SM}$, $K_{I,SM}$, $K_{D,SM}$) added to increase the dynamic performance of the torque control during transients.
In summary, the target of the PM control strategy is to guarantee a desired longitudinal vehicle speed profile, while the SM one has to satisfy a desired yaw rate by means of a controlled speed difference between the tracks.
The control logics equations adopted are:

$$\begin{cases} e_V = V_{ref} - V \\ T_{PM} = K_{P,PM} e_V + K_{I,PM} \int e_V dt + K_{D,PM} \dfrac{de_V}{dt} \\ e_{\Delta\omega} = \Delta\omega_{W,ref} - \left(\omega_{WR} - \omega_{WL}\right) \\ T_{SM} = K_{P,SM} e_{\Delta\omega} + K_{I,SM} \int e_{\Delta\omega} dt + K_{D,SM} \dfrac{de_{\Delta\omega}}{dt} + \dfrac{\hat{T}_{lL} - \hat{T}_{lR}}{\tau_{FD}\tau_{OG}\tau_{SM}\left(\sigma_{PG}+1\right)} \end{cases} \tag{41}$$

where e_V and $e_{\Delta\omega}$ are respectively the vehicle speed error and the sprocket speed difference error. The feed-forward contribution, added to increase the SM controller performance, requires the estimation of the load torque $\hat{T}_{lL}$ and $\hat{T}_{lR}$ applied to the sprockets.

4 Steady-state vehicle traction performance calculation

Under the hypothesis of negligible slip in track-terrain contact and assuming that the Steering Motor is not activated, it is possible to correlate, in first approximation, PM speed and vehicle speed, by applying eq. (15), through the following kinematic equation:

$$V_v = \frac{\sigma_{PG} R}{\tau_{AT}\,\tau_{FD}\left(\sigma_{PG}+1\right)} \omega_{PM} \tag{42}$$

where R is the sprocket radius and τ_{FD} the final drive gear ratio. In steady-state condition the same gain between the vehicle speed and PM speed can be used to obtain the vehicle

driving force, starting from the torque delivered by the electric motor; the transmission efficiency is considered unitary in this calculation.

$$F_v = \frac{\tau_{AT}\,\tau_{FD}(\sigma_{PG}+1)}{\sigma_{PG}R} T_{PM} \tag{43}$$

By using the data of the PM maximum torque map in eqs.(42) and (43) as ω_{PM} and $T_{PM}(\omega_{PM})$ and also considering the two available gear ratios of the AT, the traction diagram reported in Figure 12 can be drawn.
The vehicle load curves have been calculated regarding the three main contributions of drag: road inclination F_{incl}, rolling F_{roll} and aerodynamic F_{aero} resistance.

$$\begin{aligned} F_{drag} &= F_{incl} + F_{roll} + F_{aero} = \\ &= mg\sin\alpha + mg\left(f_0 + kV_v^{\,2}\right) + \frac{1}{2}\rho C_x S_f V_v^{\,2} \end{aligned} \tag{44}$$

where α is the road longitudinal inclination angle, f_0 and k are the rolling resistance coefficients, ρ is the air density, S_f is the vehicle frontal area and m is the vehicle mass.

5 Simulation results

The powertrain model, together with its control logic, was implemented in Matlab/Simulink® environment to evaluate both transmission and vehicle performance by numerical simulations.
Figure 13-16 present the results of a step steer simulation executed at 15 km/h with a friction coefficient between tracks and terrain of μ=0.7, equal for the longitudinal and lateral directions. The SM follows a step change in its speed of 2500 rpm that starts at second 10 of simulation time, see n_{SM} in Figure 14a. This SM speed variation determines a speed difference between the sprockets (and consequently between the tracks) and in turn a vehicle yaw rate, as shown in Figure 13b.
The PM, in the meanwhile, has to overcome, beside the rolling and aerodynamic resistances, also an additional load, that is the longitudinal component of the centrifugal force, arising from the presence of a vehicle sideslip angle during cornering. In fact, the significant longitudinal acceleration a_X, as reported in Figure 13d, has to be compensated by increasing proportionally the motor torque (see Figure 14b). The PM torque controller adjusts accordingly the torque delivered by the motor with the aim of keeping the magnitude of the vehicle speed constant during the whole turning manoeuvre. The consequent vehicle CG trajectory after the step steer is a circle of radius 7.6 m (Figure 13a). The resultant track-terrain forces are shown in Figure 15. Their longitudinal components, with opposite directions, originate the steering moment and produce the required longitudinal acceleration, while the lateral forces equilibrate the remaining component of the vehicle centrifugal force.
The main advantages given by this kind of transmission, in comparison with the purely electric two-sprocket drive, are the power saving during steering and the electric machine downsizing. The power balance of the vehicle is illustrated in Figure 16 where the power recirculation from the slow (left) to the fast (right) track, allowed by this kind of transmission, is evident. While the power supplied by the PM overcomes the rolling resistance and the aforementioned inertial term, the high power requirement of the outer

track $P_{X,R}$, due to the beginning of the step steer, is partially satisfied by the power regenerated by the inner track $P_{X,L}$, which is mechanically transferred through the lower shaft without further energy conversion, and only the extra power is taken from the SM electric motor, whose size can be therefore significantly reduced.
The steady-state power requirements of the vehicle during turning manoeuvres can be investigated through the simulation of several steps of steering motor speed while maintaining a constant vehicle speed. The values reached at the end of the simulation, when the effect of the transient response become negligible, are collected and reported in charts. As an example, Figure 17 shows the results obtained at 15 km/h. For high turning radius the power trends of the two tracks are symmetric, the regenerated power from the slow track is sufficient to satisfy the power necessary to steer the vehicle, hence the SM power contribution is negligible. The decrease of the turning radius, for a given vehicle speed, is obtained by increasing the SM speed, hence the SM has to absorb progressively more power, that can be either stored or directly utilised by the electric load of the tank. Small turning radius implies high centrifugal force and not negligible vehicle sideslip angle, the longitudinal acceleration increases and the PM has to supply more and more power. The power trends of the tracks become more asymmetric while PM power increase monotonically with the decrease of the curvature radius.

6 Conclusions

The EMT architecture presented in this paper is a series hybrid electric powertrain equipped with a zero-shaft type steering system. The model equations for both the transmission and tracked vehicle dynamics are derived starting from the respective free body diagrams. The analysis of the kinematic and dynamic EMT equations together with the presented simulation results (concerning the application of the EMT on a 53ton Main Battle Tank) of both steady-state and transient manoeuvres, allows to underline the main powertrain characteristics and gives useful information for the control strategy definition of the two electric motors. The integration of the EMT and tracked vehicle models constitutes an instrument to estimate the power flows through the transmission and the vehicle energy requirement for both propulsion and steering systems. The presented model can therefore support the electric motor size selection with relation to the vehicle's main characteristics and the desired overall dynamic performance.

References

Wong, J.Y. (2010) 'Terramechanics and Off-Road Vehicle Engineering', 2nd edition, Elsevier, ISBN: 978-0-7506-8561-0.

Hirt, M. and Naunheimer, H. (1999) 'Electro Mechanical drive system for tracked vehicles'. *Paper presented at the 4eme Congres mondial engrenages trasmissions puissance*, Paris, France, pp. 2413/2424.

Witzenberger, M. and Rothfisher, G. (2007) 'Electro-hydrodynamic superimposed steering system', Augsburg (DE), *United States Patent No.: US 7,201,691 B2.*

Task Group AVT-047 (WG-015) (2004) 'All Electric Combat Vehicle (AECV) for Future Applications', *Report of the NATO-RTO Applied Vehicle Technology Pane*

(AVT), ISBN: 92-837-1110-6.

Maclaurin, B. (2007) 'A skid steering model with track pad flexibility', *Journal of Terramechanics*, Vol.44, pp.95-110.

Maclaurin, B. (2007) 'Corrigendum to: A skid steering model with track pad flexibility', *Journal of Terramechanics*, Vol.44, pp.217-218.

Yugang, L. and Guangjun, L. (2009) 'Modeling of tracked mobile manipulators with consideration of track-terrain and vehicle-manipulator interactions', *Robotics and Autonomous Systems*, Vol.57, pp.1065-1074.

Guenter, H. H. (2007) 'Military terrain vehicles', *Journal of Terramechanics*, Vol.44, pp.23-34.

Watanabe, K., Kitano, M. and Fugishima, A. (1995) 'Handling and stability performance of a four tracked steering vehicles', *Journal of Terramechanics*, Vol.32, pp. 285-302.

Thai, T. D. and Muro, T. (1999), 'Numerical analysis to predict turning characteristics of rigid suspension tracked vehicle', *Journal of Terramechanics*, Vol.36, pp. 183-196.

Figure 1 The powertrain block diagram

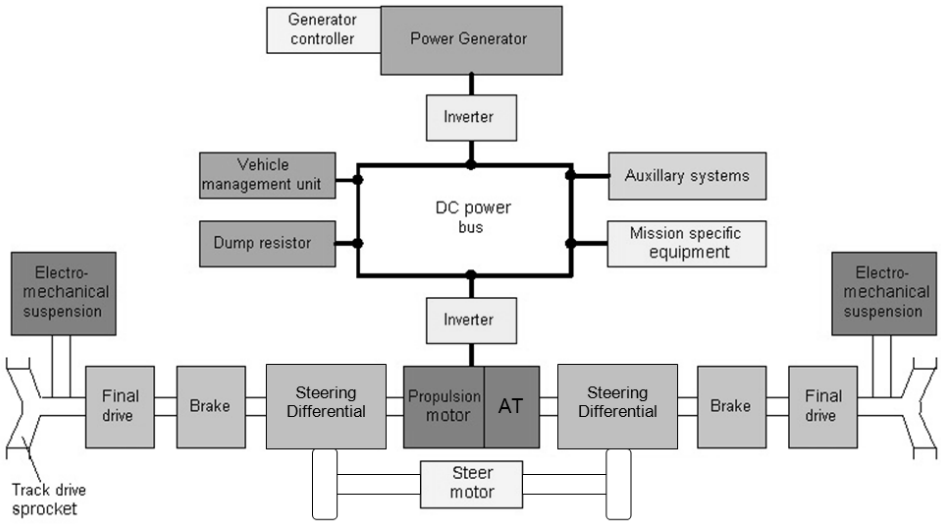

Figure 2 Stick diagram of the EMT

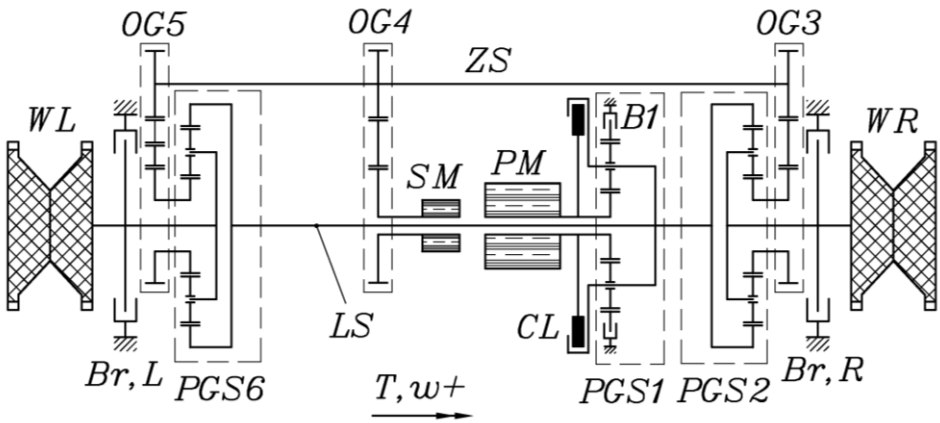

Table 1 Forward drive ranges of the two-speeds AT

Drive range	*Clutch*	*Brake*	*Gear ratio (τ_{AT})*
Neutral	Off	Off	-
1	Off	On	3.3
2	On	Off	1

Figure 3 The main structure of the tracked tank dynamic model

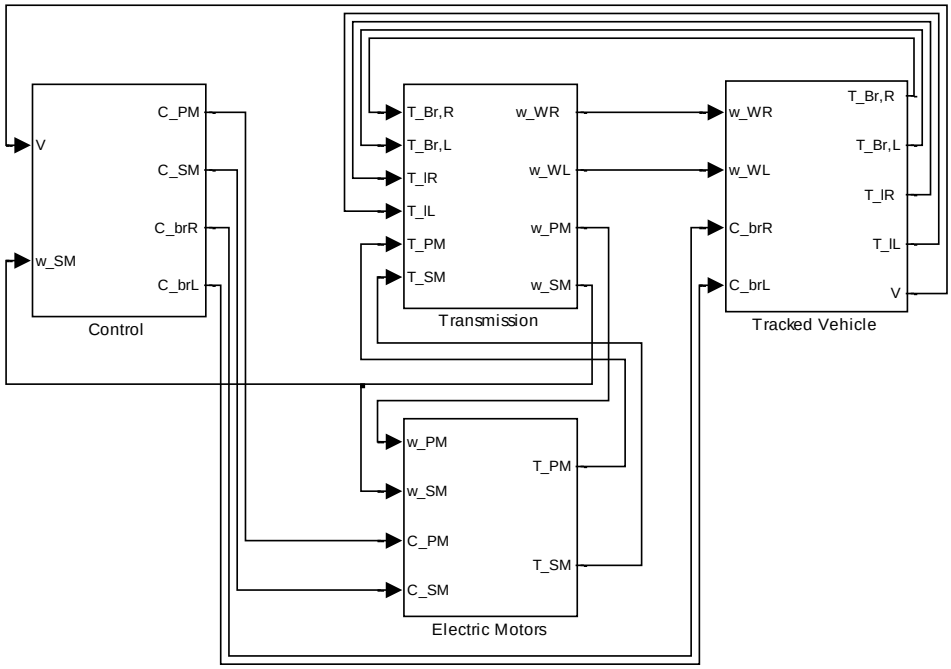

Figure 4 Driveline free body diagrams

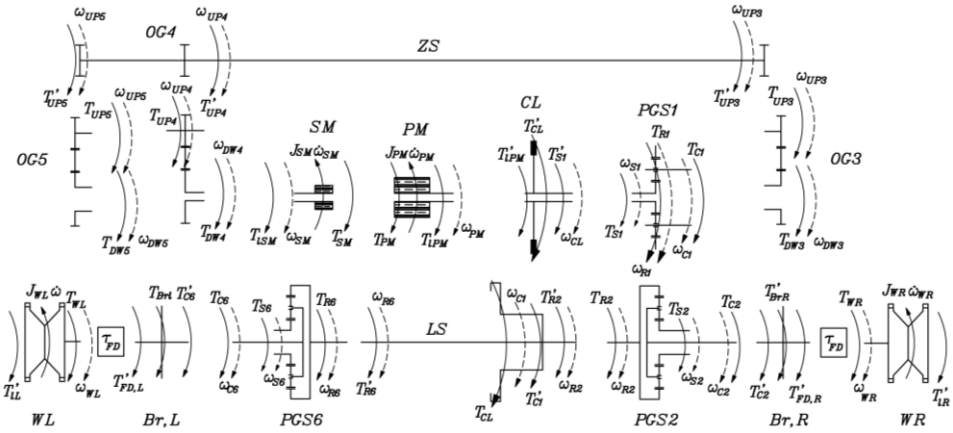

Figure 5 Free body diagram of the tracked tank (top view)

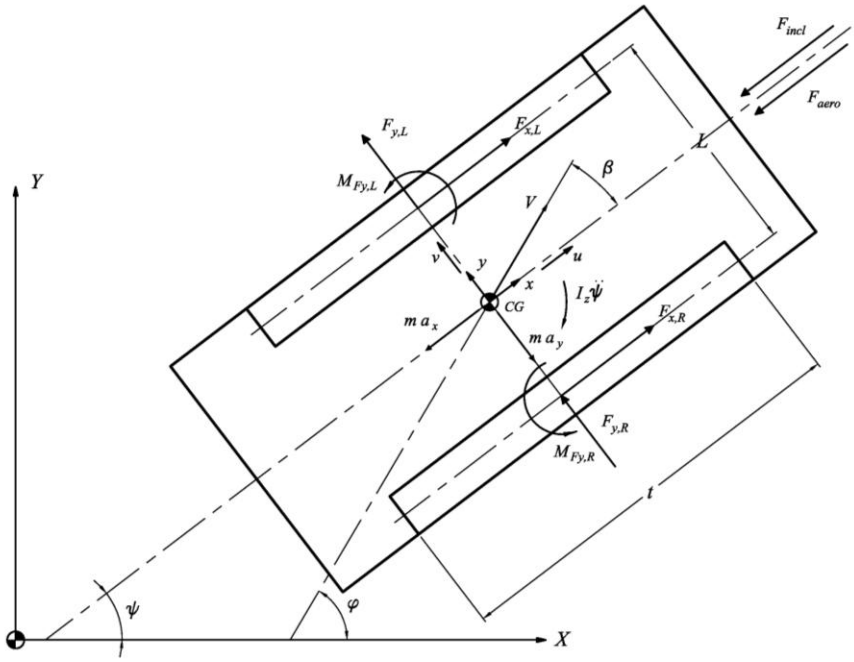

Figure 6 Longitudinal force as a function of longitudinal slip (on the left) and lateral force as a function of sideslip angle (on the right) used for each contact patch.

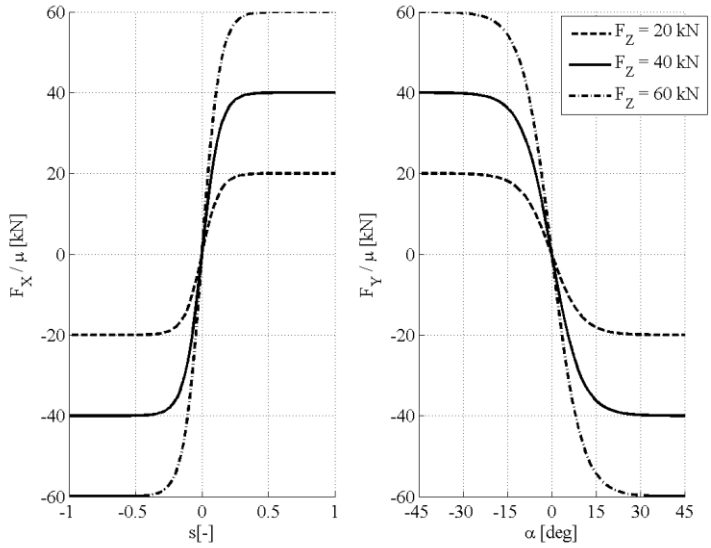

Figure 7 Lateral force vs. longitudinal force for different sideslip angles and longitudinal slips

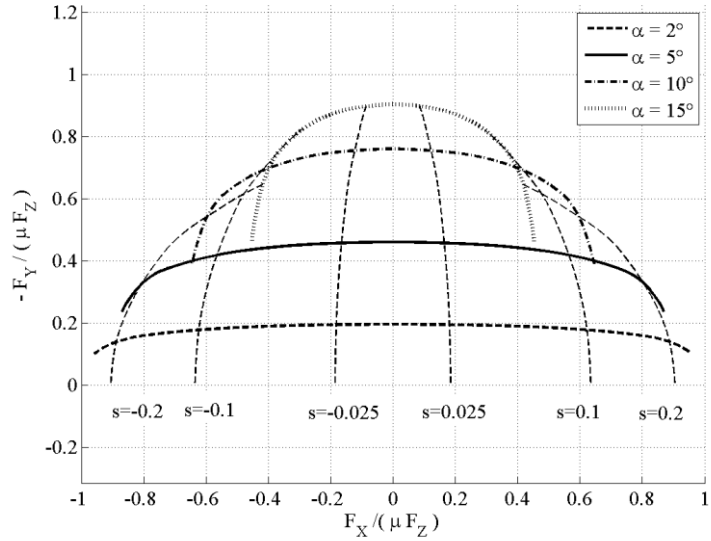

Figure 8 Track-terrain discretised contact model

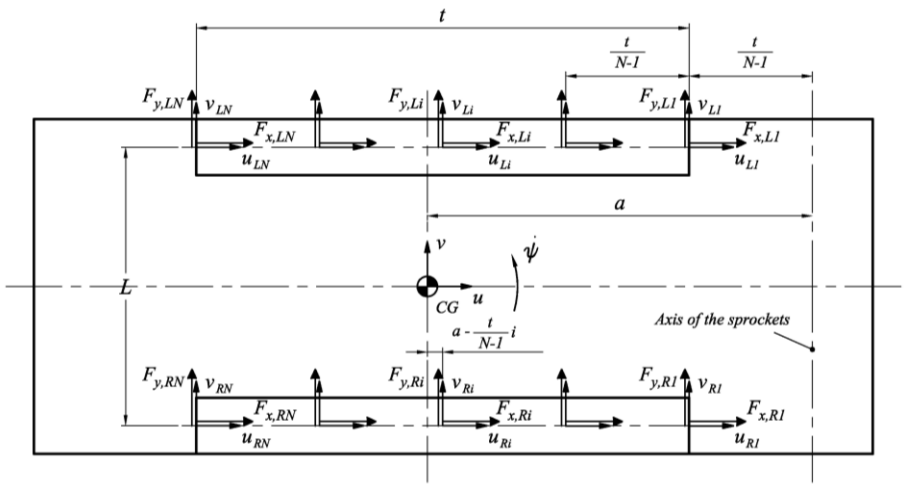

Figure 9 Rear (a) and lateral (b) view of tracked tank for lateral and longitudinal weight transfer computation.

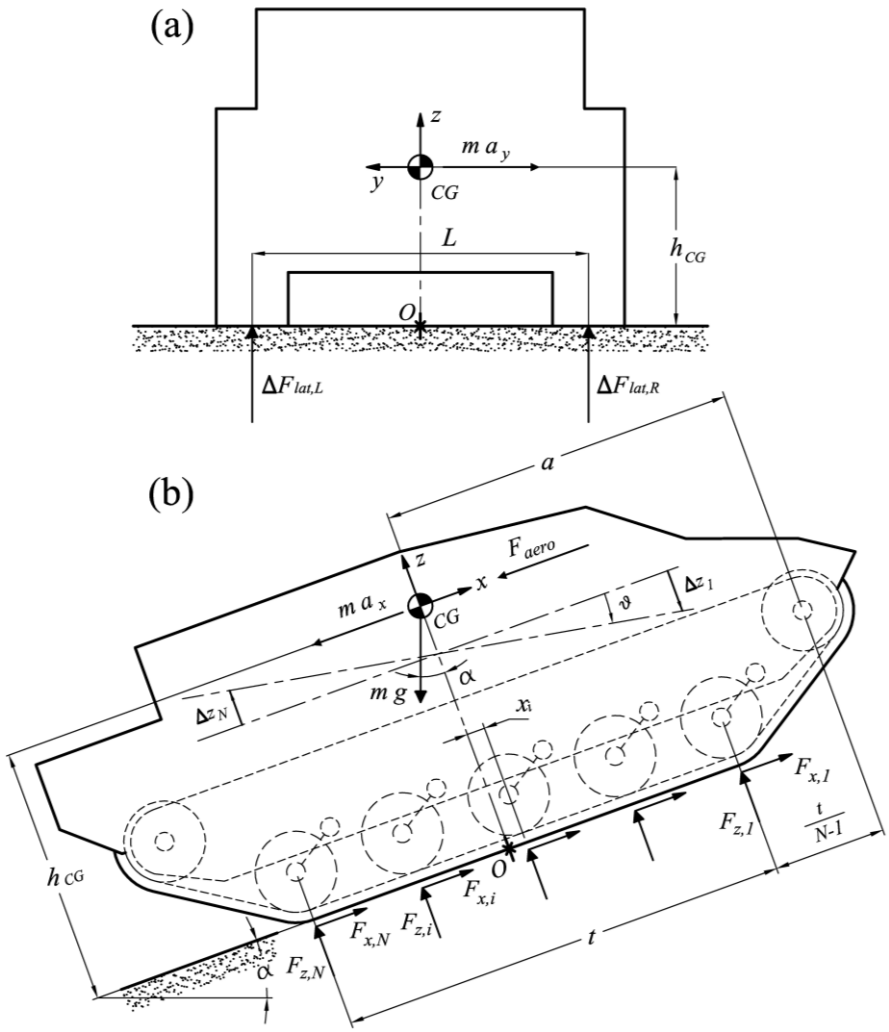

Figure 10 Tracked vehicle suspension

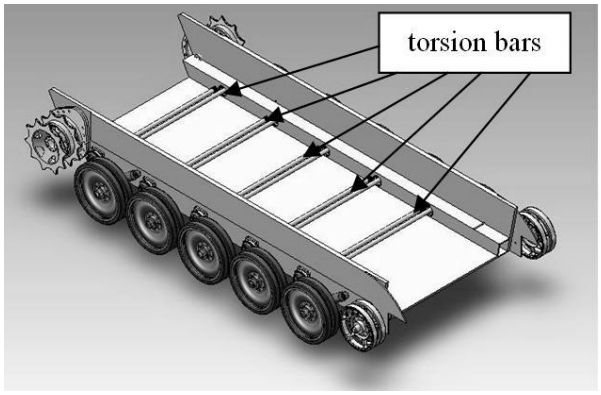

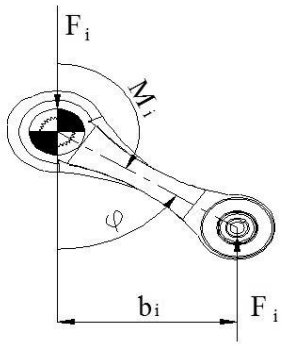

Figure 11 Torque and power steady-state characteristics of propulsion (PM) and steering (SM) motors

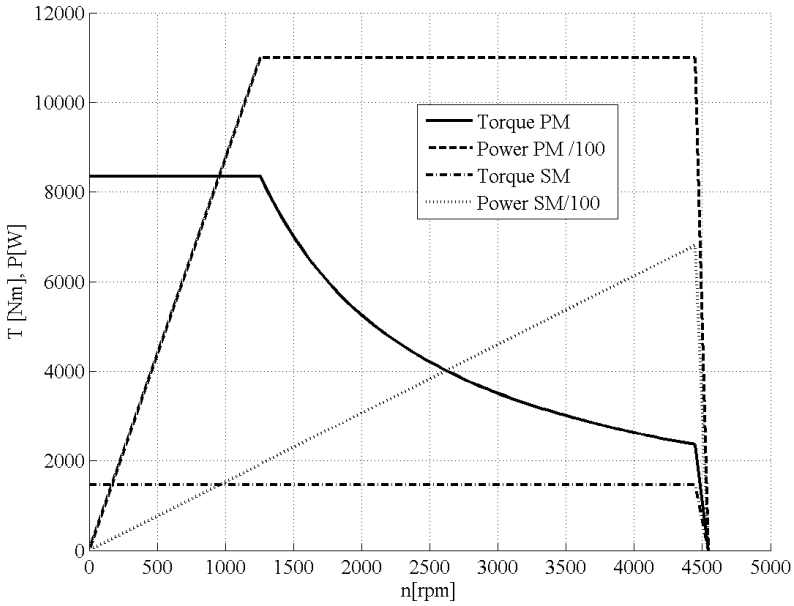

Figure 12 Longitudinal performance expected from the MBT equipped with the EMT

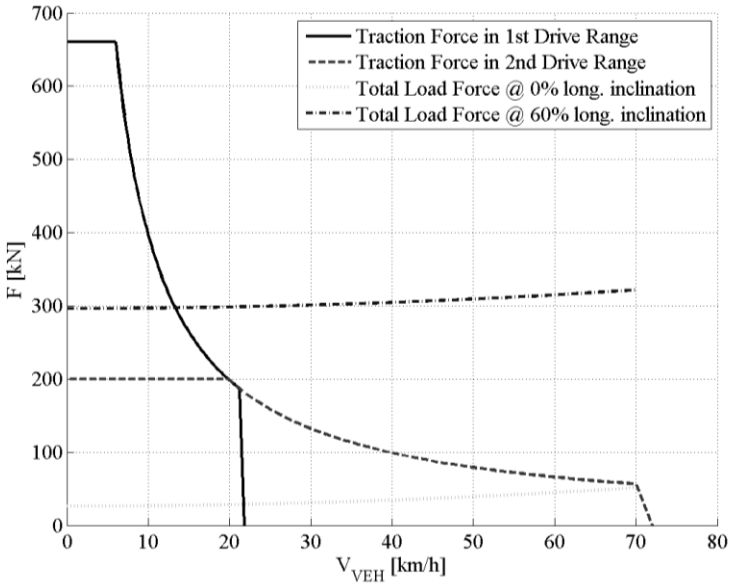

Figure 13 Transient response to a step steer input at 15 km/h: (a) Tank CG trajectory, (b) yaw rate, (c) sideslip angle and (d) longitudinal and lateral accelerations.

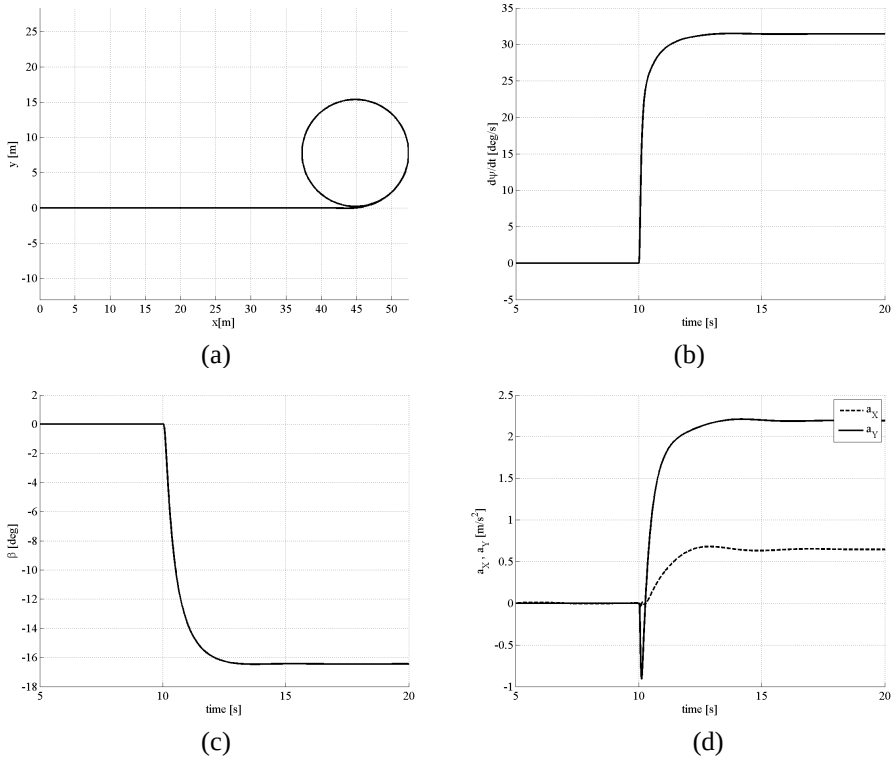

Figure 14 Transient response to a step steer input at 15 km/h. (a) EMT Speeds: propulsion motor speed (n_{PM}), steering motor speed (n_{SM}), sprocket speeds (n_L and n_R) and vehicle speed (V_{veh}); (b) EMT Torques: propulsion motor torque (T_{PM}) and steering motor torque (T_{SM}).

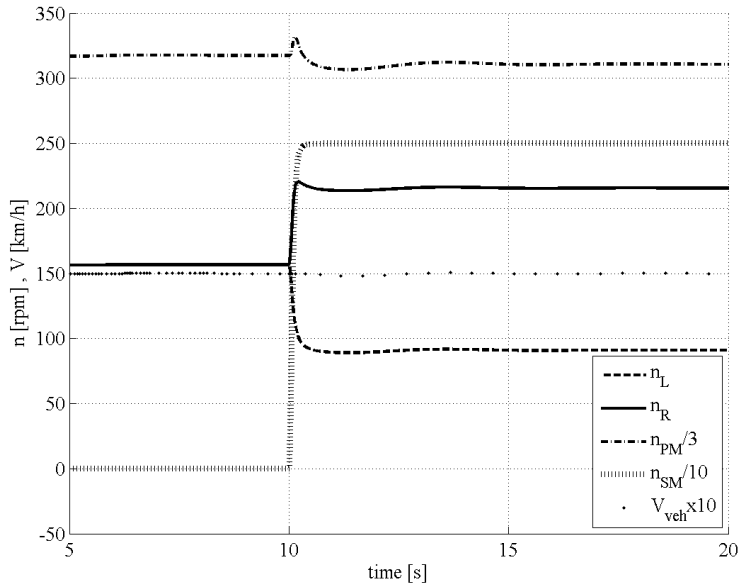

(a)

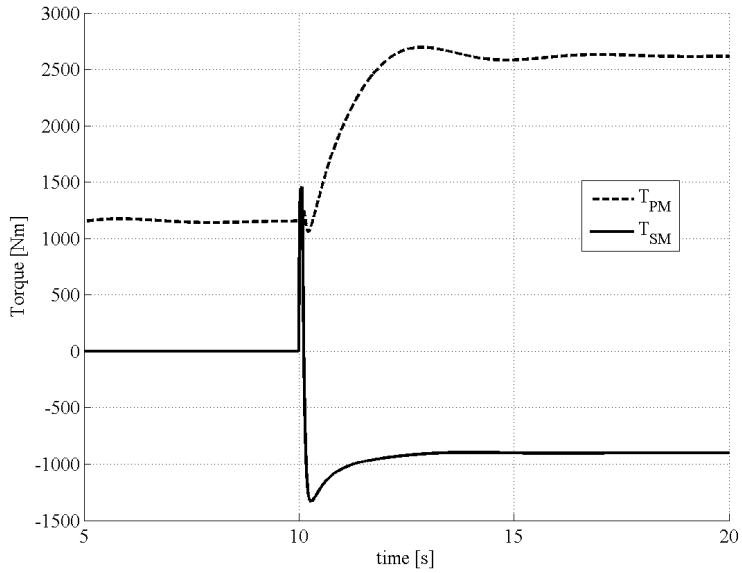

(b)

Figure 15 Transient response to a step steer input at 15 km/h: the resultant longitudinal ($F_{X,L}$ and $F_{X,R}$) and lateral forces ($F_{Y,L}$ and $F_{Y,R}$) exchanged between tracks and terrain.

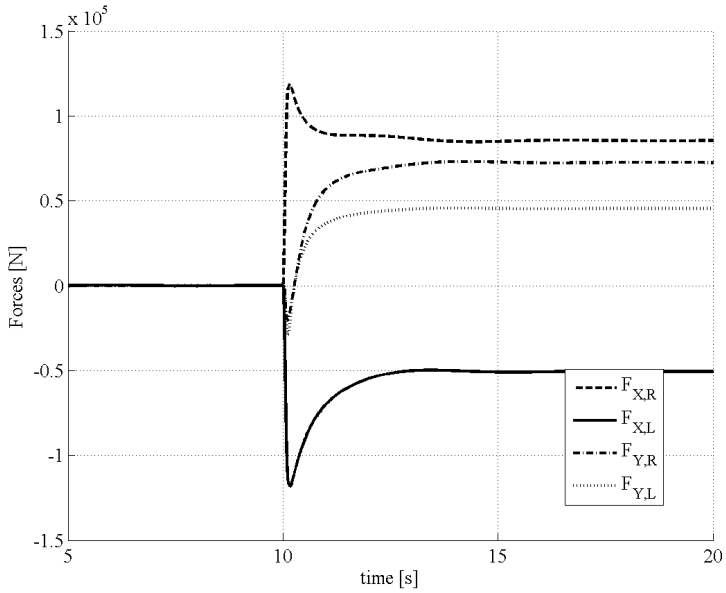

Figure 16 Transient response to a step steer input at 15 km/h: power delivered by the propulsion motor (P_{PM}) and by the steering motor (P_{SM}), power loss due to rolling resistance ($P_{Roll.Res.}$), power due to track-terrain interaction ($P_{X,R}$ and $P_{X,L}$).

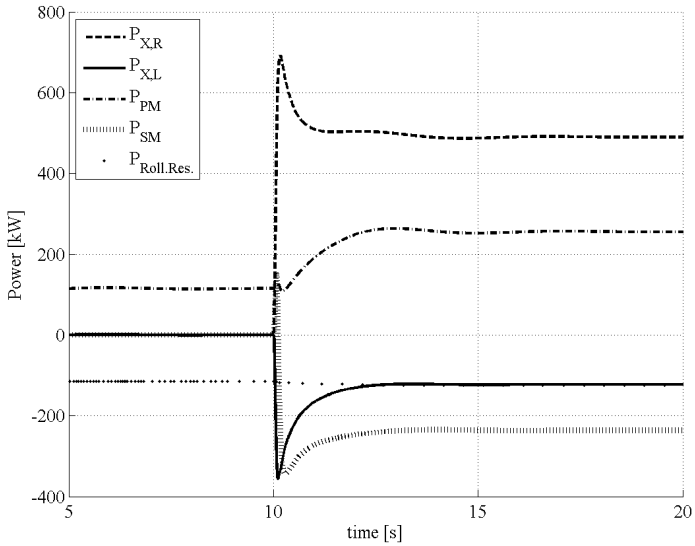

Figure 17 Power requirements of the tracked tank during steady-state turning manoeuvres at 15 km/h.